Motional stability of the quantum kicked rotor: A fidelity approach

F. Haug, M. Bienert, and W. P. Schleich
Abteilung für Quantenphysik, Universität Ulm, D-89069 Ulm, Germany

T. H. Seligman
Centro de Ciencias Físicas, University of Mexico (UNAM), C.P. 62210 Cuernavaca, Mor. Mexico

M. G. Raizen
Center for Nonlinear Dynamics and Department of Physics, The University of Texas at Austin, Austin, Texas 78712-1081, USA
(Received 16 July 2004; published 5 April 2005)

We propose an atom optics experiment to measure the stability of the quantum kicked rotor under perturbations of the Hamiltonian. We avail ourselves of the theory of Loschmidt echoes, i.e., we consider the overlap of a quantum state evolved in a perturbed and an unperturbed potential. Atom interferometry allows us to determine the overlap integral in amplitude *and* phase. A numerical analysis of the kicked rotor in various regimes shows that the quantum signatures of specific classical properties can be detected experimentally.

DOI: 10.1103/PhysRevA.71.043803 PACS number(s): 42.50.Ct, 05.45.Mt, 39.20.+q, 42.50.Vk

I. INTRODUCTION

In the controversy between Loschmidt and Boltzmann concerning the time reversibility in thermodynamics [1], echo dynamics has played a central role. Around the same time similar considerations were made independently by Lord Kelvin [2]. During the last decades the idea of echo dynamics was adopted in the field of quantum chaos to investigate the stability of quantum motion. Since then, a wealth of striking phenomena have emerged [3–11]. In the present paper we show that relevant signatures of echo dynamics for the kicked rotor, a paradigm of quantum chaos [12], can be measured with state-of-the-art technology of quantum optics.

The rapidly expanding field of quantum chaos analyzes the fingerprints of classical chaos in quantum systems. In classical systems the Lyapunov exponent allows us to distinguish two radically different types of motion, the regular motion of integrable systems and the chaotic motion of nonintegrable systems. Such a classification is based on trajectories in phase space where the Lyapunov exponent is a measure for the spreading of a bundle of adjacent trajectories originating from slightly different initial conditions. In contrast, the concept of phase-space trajectories becomes meaningless in quantum systems for times larger than the Ehrenfest time. Only up to this time the system behaves essentially classically and features such as the Lyapunov exponent are relevant [5,6,13,14].

Due to the intrinsic linearity of quantum-mechanics sensitivity to variations of initial conditions is absent. Therefore considerable interest in testing sensitivity to perturbations of the Hamiltonian has emerged. These studies have mainly focused on the fidelity in echo dynamics [3–11,14–16], although other concepts have been used [17–19]. Experiments have been carried out as early as 1950 in nuclear magnetic resonance [20–22]. Moreover, theoretical proposals have been put forward using ion traps [23] and experiments performed in atom optics [24]. Another experiment using electromagnetic billiards [25] is in progress.

In this paper we concentrate on the model of the kicked rotor [26,27]. Its classical dynamics given by the standard map [12] displays regimes from integrability to near complete chaos. In the quantum case it shows typical signatures of quantum chaos such as suppression of classical diffusion also known as dynamical localization [28]. The kicked rotor has become even more attractive since its atom optical realization [29] has opened a promising experimental testing ground [30–32].

We apply the theory of Loschmidt echoes to the kicked rotor and compare the cases of classically chaotic and regular dynamics. Moreover, we suggest a possible experimental setup for the measurement of the fidelity of the quantum kicked rotor. Thereby we exploit atom interferometry [23,24,33] to propose a measurement of the Loschmidt echo. Our scheme is based on the dynamics of a coherent superposition of two atomic hyperfine states propagating in two slightly different optical potentials. The readout provides the real and imaginary part of the quantum-mechanical overlap integral, i.e., fidelity amplitude. We emphasize that the proposed atom optical realization for the measurement of the fidelity decay requires only state-of-the-art technologies. Our numerical analysis constitutes preparatory work for possible experiments and yields deeper theoretical insight into the dynamics of the kicked rotor. So far, echo dynamics has only been studied [8] in the semiclassical limit for chaotic situations.

Our paper is structured as follows: In Sec. II we review the model of the quantum kicked rotor and summarize its time evolution. Section III serves as an introduction into the theory of Loschmidt echoes in the regime of linear response and beyond. The results of our numerical analysis are presented in Sec. IV in detail. Section V is dedicated to the discussion of a possible atom optical measurement of the fidelity for the kicked rotor. Finally, we conclude with Sec. VI.

II. KICKED ROTOR

In order to lay the foundations for the stability analysis in the following sections, we now briefly summarize the basics of the kicked rotor. In particular, we define the Hamiltonian as well as the Floquet operator describing the stroboscopic time evolution.

A. Hamiltonian

We consider a particle with mass M periodically kicked by a sine potential with wave number k_0 and amplitude $\hbar\kappa$. Thus the time evolution of the quantum state $|\psi\rangle$ is determined by the Hamiltonian

$$\hat{H} = \frac{\hat{p}^2}{2M} + \hbar\kappa \sin(k_0\hat{x})\,\delta_T(t), \tag{1}$$

where the kicks are modeled by a series of delta functions,

$$\delta_T(t) = \sum_{n=-\infty}^{\infty} \delta(t/T - n) \tag{2}$$

with temporal separation T. For the case of periodic boundary conditions the Hamiltonian, Eq. (1), describes the drosophila of quantum chaos, the kicked rotor.

It is convenient to introduce the dimensionless coordinate $\theta = k_0 x$ and the momentum $\rho = (k_0 T/M)p$ which fulfill the commutation relation $[\theta,\rho] = i\hbar$ with the scaled Planck constant $\hbar = \hbar(k_0^2 T/M)$. Furthermore, we use the scaled time $N = t/T$ where the integer N counts the number of kicks. Consequently, we find the new Hamiltonian,

$$\hat{\mathcal{H}} \equiv \hat{T} + \hat{V}(\hat{\theta},N) = \frac{\hat{\rho}^2}{2} + K \sin\hat{\theta}\,\delta_1(N),$$

consisting of the kinetic energy $\hat{T}$ and the potential $\hat{V}(\hat{\theta},N)$, with kick strength $K = \hbar\kappa(k_0^2 T^2/M)$, and according to Eq. (2), we have $\delta_1(N) = \Sigma_n \delta(N-n)$. In the classical limit we find for $K < 1$ a globally stable phase space whereas for $K \gg 1$ the phase space is near globally chaotic.

B. Time evolution

We now turn to the time evolution. Due to the stroboscopic kicks with the potential V we reduce the continuous time evolution to a discrete map. Between two kicks the potential vanishes and the state $|\psi_N\rangle$ evolves freely according to $|\psi_N'\rangle = \hat{U}_{\text{free}}|\psi_N\rangle$ with $\hat{U}_{\text{free}} \equiv \exp[-i\hat{\rho}^2/(2\hbar)]$. Only for integer times N the potential energy dominates the kinetic energy and we can omit the latter, i.e., the kick transforms the state according to $\hat{U}_{\text{kick}}|\psi_N'\rangle$ with $\hat{U}_{\text{kick}} \equiv \exp[-iK\sin\hat{\theta}/\hbar]$. Hence the state $|\psi_{N+1}\rangle$ immediately after the $(N+1)$st kick is related to the state $|\psi_N\rangle$ by the map

$$|\psi_{N+1}\rangle = \hat{U}|\psi_N\rangle$$

with the Floquet operator $\hat{U} \equiv \hat{U}_{\text{kick}}\hat{U}_{\text{free}}$. Consequently, the state after N kicks is connected to the initial state $|\psi_0\rangle$ via

$$|\psi_N\rangle = \hat{U}^N|\psi_0\rangle. \tag{3}$$

We conclude this section by presenting the Floquet operator $\hat{U}$ in the basis of the unperturbed momentum eigenstates $|\rho\rangle$ which fulfill the eigenvalue equation $\hat{\rho}|\rho\rangle = \rho|\rho\rangle$. Since we deal with periodic boundary conditions we have a discrete spectrum $\rho = l\hbar$ of the momentum operator. Thus we find $|\rho\rangle = |l\hbar\rangle$ with $l = 0, \pm 1, \pm 2, \ldots$. Therefore in the momentum basis $|l\hbar\rangle$ the Floquet operator reads

$$\hat{U} = \sum_{l,l'} e^{-i(l^2\hbar/2)}\langle l'\hbar|\hat{U}_{\text{kick}}|l\hbar\rangle|l'\hbar\rangle\langle l\hbar|, \tag{4}$$

where the matrix elements are simply given by a Bessel function $\langle l'\hbar|\hat{U}_{\text{kick}}|l\hbar\rangle = J_{l-l'}(K/\hbar)$.

III. ECHO DYNAMICS

The idea of echo dynamics is to evolve an initial state from $t=0$ to $t=T$ with the Hamiltonian $\hat{H}$ and subsequently backwards with a slightly perturbed Hamiltonian $\hat{H}'$. A comparison of the echo state with the initial state might serve as a criterion for the stability of the system under perturbation of the Hamiltonian.

A. Fidelity

For the quantum case the standard measure to compare the initial state $|\psi_0\rangle$ with the echo evolved state $|\tilde{\psi}\rangle$ is the fidelity

$$\mathcal{F} \equiv |f|^2 \equiv |\langle\psi_0|\tilde{\psi}\rangle|^2, \tag{5}$$

where the fidelity amplitude f measures the complex-valued overlap between the two states.

We now apply echo dynamics to the kicked rotor. Recalling Eq. (3) leads to $|\tilde{\psi}\rangle = [\hat{U}\hat{U}_\delta]^{-N}\hat{U}^N|\psi_0\rangle$ with $\hat{U}_\delta = \exp[-i\delta\sin\hat{\theta}/\hbar]$, i.e., we use a perturbed potential with amplitude $K+\delta$, where we assume δ to be a small perturbation. To this end we insert the expression for $|\tilde{\psi}\rangle$ into the definition of the fidelity, Eq. (5), and finally find

$$\mathcal{F}_N = |f_N|^2 = |\langle\psi_0|[\hat{U}\hat{U}_\delta]^{-N}\hat{U}^N|\psi_0\rangle|^2 \equiv |\langle\phi_N|\psi_N\rangle|^2. \tag{6}$$

We emphasize that this expression can be reinterpreted as the overlap between the forward propagated states $|\psi_N\rangle \equiv \hat{U}^N|\psi_0\rangle$ and $|\phi_N\rangle \equiv [\hat{U}\hat{U}_\delta]^N|\psi_0\rangle$ starting both from the same initial state $|\psi_0\rangle$.

B. Linear response and beyond

Since the perturbation δ is assumed to be small with regard to all other parameters, it stands to reason to treat the problem perturbatively with δ as the smallness parameter. A detailed general analysis of this problem was already worked out by Prosen and co-workers [7] and in the linear-response regime the fidelity reads

$$\mathcal{F}_N = 1 - \frac{\delta^2}{k^2} \sum_{\mu,\nu=0}^{N-1} \overleftarrow{T} \mathcal{C}_{\mu,\nu} + \mathcal{O}(\delta^3). \tag{7}$$

For the kicked rotor the two-time correlation function

$$\mathcal{C}_{\mu,\nu} \equiv \langle \psi_0 | \sin \hat{\theta}_\mu \sin \hat{\theta}_\nu | \psi_0 \rangle$$

involves the time-dependent position operator $\hat{\theta}_\nu \equiv \hat{U}^{-\nu} \hat{\theta} \hat{U}^{\nu}$ in the interaction picture. Moreover, the time ordering operator $\overleftarrow{T}$ accounts for the noncommutativity of the operators at different times μ and ν.

Equation (7) shows clearly that the behavior of the fidelity as a function of the kick number is solely determined by the two-time correlation function $\mathcal{C}_{\mu,\nu}$ whereas δ and k are scaling parameters. Consequently, the fidelity reflects the distinct characteristics of this correlation function in the classically integrable and chaotic regimes. The further analysis makes use of these differences in order to find simpler expressions for the fidelity.

1. Chaotic case

In the classically chaotic regime [47] we can assume that for times larger than the Ehrenfest time τ_E, that is, when an initial wave packet has spread over the whole phase space, the correlation function becomes independent of the initial state. This assumption implies that the correlation function depends only on the time difference—or in our case the difference $\mu - \nu$ in the number of kicks. If we additionally assume that the correlation function decays sufficiently fast for increasing $|\mu - \nu|$, we find in the linear-response regime the compact expression

$$\mathcal{F}_N^{\text{chaos}} = 1 - 2\frac{\delta^2}{k^2} \widetilde{\mathcal{C}} N, \tag{8}$$

where the constant $\widetilde{\mathcal{C}}$ can be calculated from the correlation function $\mathcal{C}_{\mu,\nu}$. Its explicit form is given in Ref. [7].

This analysis can be extended beyond the linear-response regime by heuristically assuming Eq. (8) to represent the first two terms of an exponential,

$$\mathcal{F}_N^{\text{chaos}} = \exp\left[- 2\frac{\delta^2}{k^2} \widetilde{\mathcal{C}} N \right]. \tag{9}$$

For the case of Gaussian statistics of the two-time correlation function, this result is exact. Even for non-Gaussian statistics this approximation can be extremely accurate [10].

2. Integrable case

In the classically integrable case we find a different behavior since the time average of the correlation function converges to a constant $\overline{\mathcal{C}}$. Using this characteristic property together with Eq. (7) we arrive at a quadratic time decay

$$\mathcal{F}_N^{\text{int}} = 1 - \frac{\delta^2}{k^2} \overline{\mathcal{C}} N^2. \tag{10}$$

As in the nonintegrable case, we can extend this expression to a Gaussian decay

$$\mathcal{F}_N^{\text{int}} = \exp\left[- \frac{\delta^2}{k^2} \overline{\mathcal{C}} N^2 \right], \tag{11}$$

which can be exact in many semiclassical situations [7,34].

Note, that the results, Eqs. (10) and (11), are in direct contradiction [7] with the original work of Peres [4]. Indeed, this fact gave rise to plenty of confusion and false conclusions. We emphasize that integrable systems have no *generic* behavior, and therefore fidelity will depend in a more sensitive way on the initial state. In other words, the decay of correlations might be quite atypical for particular states. Moreover, the harmonic component of a stable island stabilizes the quantum motion of coherent states near the center of this island, as we shall see in Fig. 8. Indeed, Peres used a coherent state in the very center of an island, and thus obtained results quite atypical for integrable systems in general. Even if we average over a fixed set of orthogonal states, the dependence on the choice of this set may still be very strong as pointed out by Ref. [35]. Only random states in anharmonic integrable systems will display something akin to a *generic* behavior. However, random states go beyond the scope of the present paper since they are of little interest for the proposed experiment.

In the next section we test numerically the scaling behavior of Eqs. (8) and (10) as well as the validity of Eqs. (9) and (11) for different values of K corresponding to the chaotic and integrable regime.

IV. NUMERICAL ANALYSIS

We now turn to our numerical simulations and investigate the behavior of the fidelity as a function of the kick number. We start mostly with single momentum eigenstates but consider also Gaussian packets in momentum space and mixed states. We first focus on the chaotic and near-integrable cases and then present the case of mixed dynamics sometimes referred to as soft chaos.

We illustrate the results of our simulations using a phase space spanned by the coordinate θ and the momentum ρ. Momentum eigenstates $|lk\rangle$ with $l = 0, \pm 1, \pm 2, \ldots$ are represented as a uniform distribution of area $2\pi k$ in phase space what reflects the uncertainty relation between θ and ρ. It has an extension in the ρ direction of k centered around the value lk.

For the simulations of fidelity decay we choose the perturbation strength $\delta = 0.02$ in all figures, as similar values are correctly related by the scaling properties Eqs. (8) and (10).

A. Chaotic case

In order to be in the globally (near) chaotic regime we choose $K = 10$. Figure 1(a) displays the global structure of phase space in a Poincaré plot. No stable islands can be seen.

1. Momentum eigenstates

We chose two initial momentum eigenstates with $l = 0$ and $l = 16$, respectively, and $k = 0.15$. In Fig. 1(a) we have shaded the area occupied by the initial momentum eigenstate. In Figs. 1(b) and 1(c) we show the fidelity $\mathcal{F}_N$ as a function of

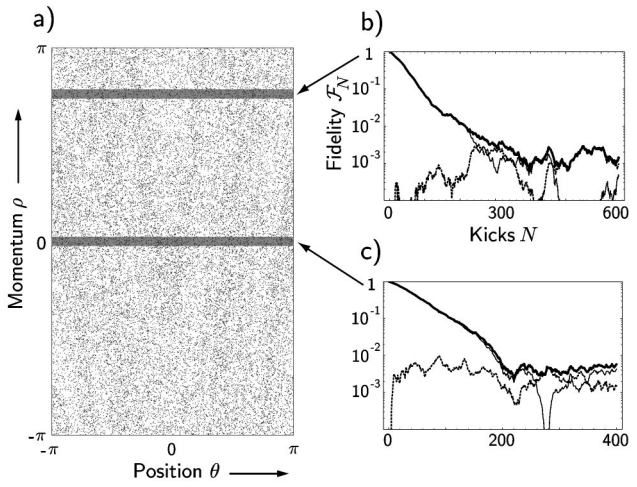

FIG. 1. Fidelity decay in the nonintegrable case. In (a) the Poincaré plot of the classical phase space is shown for $K=10$. Since this corresponds to a globally chaotic regime no stable island is visible. The shaded regions denote phase-space representations of the momentum eigenstates $|\rho=0\rangle$ and $|\rho=16\hbar\rangle$. The decay of the fidelities corresponding to these two initial states are shown in (b) and (c). The thick line depicts the fidelity $\mathcal{F}_N$ whereas the thin line represents the square of real part of the fidelity amplitude f_N and the dotted line the square of the imaginary part, respectively. The parameters are $K=10$, $\hbar=0.15$, and $\delta=0.02$.

the kick number N on a semilogarithmic scale. For both initial states the fidelity decays exponentially in the beginning but saturates after a certain number of kicks and fluctuates around a mean plateau. The homogeneity of the Poincaré plot explains their similar behavior. This decay of the fidelity $\mathcal{F}_N$ is in good agreement with the theoretical predictions presented in Sec. III. The plateau is due to dynamical localization, as we shall see later.

In addition to the fidelity $\mathcal{F}_N$, we also display the square of the real and imaginary parts $(\mathrm{Re}\, f_N)^2$ and $(\mathrm{Im}\, f_N)^2$ of the fidelity amplitude f_N since our proposed experiment allows a measurement of both of this quantities. Whereas the real part determines the short-time behavior of fidelity, the plateau is due to both parts.

2. Mixed states

In order to average out the fluctuations in the fidelity we use an uniform incoherent superposition of many momentum eigenstates as initial state. This approach allows us a quantitative comparison with the approximate analytic expressions and the ensuing scaling laws. The results for $\hbar=0.05$, $\hbar=0.075$, $\hbar=0.125$, and $\hbar=0.2$ are plotted in Fig. 2.

Again we recognize the exponential decay of the fidelity but the fluctuations are now smoothed and clearly defined plateaus emerge. For $\hbar=0.2$ on the other hand we find a notable deviation from linear decay at short times. One might suspect that this deviation from linear behavior is a manifestation of the Zeno effect, since for a small number N of kicks and for the case that the correlation function $\mathcal{C}_{\mu,\nu}$ can be assumed to be constant in this regime, we get $\mathcal{F}_N \approx 1 - (\delta^2/\hbar^2)\mathcal{C}_{0,0}N^2$. However, the time scale of this effect is far too short to explain this result. We thus have to conclude that the correlation function decays more slowly than expected and we have checked numerically that this is indeed the case. While this anomaly is not understood in full detail, it is clear that exponential decay originates from the fact, that the correlation function decays to zero. Yet a finite dimensional Hilbert space creates some residual correlations. This causes a Gaussian decay, which always competes with the exponential one. For very large Hilbert spaces, however, it will become quite insignificant. Dynamical localization restricts this dimension. For large enough values of the effective Planck's constant this Gaussian decay will dominate the exponential one. We wish to point out that the anomalously long correlations found in the chaotic regime are in the range of effective $\hbar$ values which are in an experimentally feasible domain.

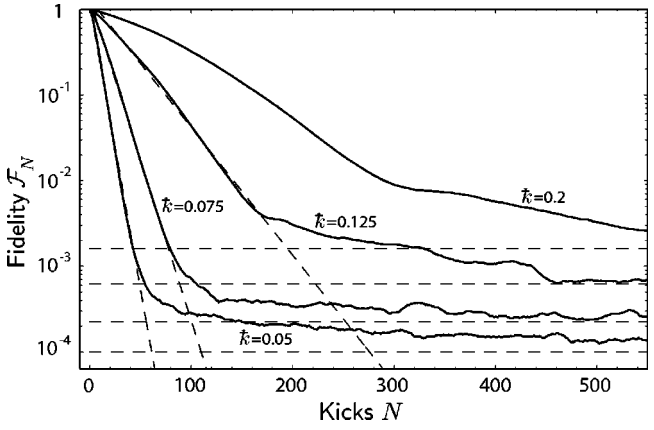

FIG. 2. Fidelity decay averaged over many different momentum eigenstates in the nonintegrable regime. The curves show an exponential behavior as predicted by Eq. (9) except of the plot corresponding to $\hbar=0.2$. This discrepancy is not explained by the theory of Sec. III B and is a consequence of dynamical localization. We have fitted the exponential functions to the range where the exponential decay occurs. The fidelity saturates due to the effectively finite size of the Hilbert space. The dashed horizontal lines mark the position of the resulting plateaus $\mathcal{F}_\infty$. We chose again $K=10$ and $\delta=0.02$.

We fit exponentials $\beta \exp[-N/\alpha(\hbar)]$ to the near linear part of the curves. To test the scaling law with respect to $\hbar$ we consider the pairwise ratio of the slopes. When we assume an essentially $\hbar$-independent correlation function $\tilde{\mathcal{C}}$ we expect from Eq. (9) a ratio of 2.25 and 2.78 for the pairs $\hbar=0.05$ and $\hbar=0.075$, respectively, $\hbar=0.075$ and $\hbar=0.125$. The corresponding ratios following from the fits are 1.87 and 2.52. Both numerically determined ratios are below the theoretical counterparts. This discrepancy reflects the fact that after many kicks linear response is no longer exact. In particular, we find that for growing smallness parameter $(\delta/\hbar)^2$ the deviation becomes larger. Moreover, for our theoretical estimations we have neglected the $\hbar$ dependency of the correlation function.

We note that we have also checked the fidelity decay for Gaussian-like initial states and found that the results do not considerably differ from the incoherent superpositions shown in Fig. 2. This can be understood since due to the completely structureless phase space the fidelity does not depend on the initial state.

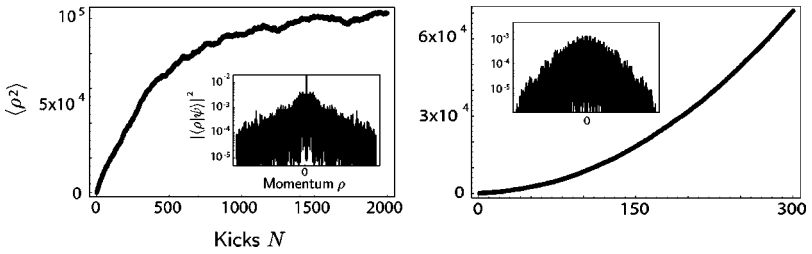

FIG. 3. Mean energy of the kicked rotor as function of the kick number N for dynamical localization (left) and for a quantum resonance (right). In the case of localization (left) the mean energy starts to grow linearly analogously to the classical diffusion, but for larger kick numbers it diverges from the linear growth and turns into an oscillatory, bounded behavior. For the left figure we have chosen $\hbar=0.15$. However, for a slightly different $\hbar=4\pi/100=0.125\,663\,7\cdots$ we are on a quantum resonance (right). Here, the mean energy shows an almost perfect quadratic growth. In the insets we have plotted the momentum distribution of the state $|\psi_N\rangle$ after $N=2000$ (left) and $N=300$ (right) kicks in a logarithmic scale. While the exponential decay as a typical indication for localization is clearly visible on the left, the decay is clearly nonexponential on the right. The latter indicates that for quantum resonances the system does not localize. For both plots we have used the parameter $K=10$ and the initial state $|\rho=0\rangle$.

3. Plateau

In order to understand the appearance of the plateaus we recall the phenomenon of dynamical localization [28]. After a certain number of kicks the state $|\psi_N\rangle$ reaches its largest extension in momentum space and does not grow any further [27,36,37]. The localization length L estimated [38] by

$$L = \frac{K^2}{4\hbar^2} \tag{12}$$

determines the effective dimension of Hilbert space.

For the chosen parameter range the kicked rotor exhibits dynamical localization as shown in Fig. 3.

According to Ref. [7] the height of the plateau is given by the inverse of the Hilbert space dimension. We assume that due to the localization the effective dimensionality is determined by L, Eq. (12), and thus we expect the plateaus to emerge at

$$\mathcal{F}_\infty = 4\hbar^2/K^2.$$

The theoretical plateaus $\mathcal{F}_\infty$ for the curves shown in Fig. 2 are represented by dashed horizontal lines and show good agreement with the numerical results supplying the assumption that the dynamical localization influences strongly the behavior of the fidelity decay.

4. Quantum resonances

So far we have considered parameters where the system exhibits dynamical localization. We now consider values of $\hbar$ where quantum resonances appear. For $\hbar=4\pi$ the phase factor in the Floquet operator, Eq. (4), describing the free time evolution between two kicks vanishes and $\hat{U}$ is simply given by $\hat{U}_{\text{kick}}$. Therefore all kicks are in phase and add up coherently leading to a quadratic growth in energy. In fact also for $\hbar=4\pi(p/q)$ with p and q are mutually prime integers we find a asymptotically quadratic dependence [39] of energy due to constructive quantum interference. Figure 3 shows that even for the resonance $p=1$ and $q=100$ leading to $\hbar=0.125\,663\,7\cdots$ the quadratic growth is clearly visible.

Figure 4 shows the fidelity decay for the case of a quantum resonance. The result—a Gaussian decay—is in sharp contrast to the exponential decays depicted in Figs. 1(b) and 1(c). This behavior results from the pure quantum origin of the resonances. In fact, they are a result of constructive interference and can be interpreted as kicked fractional revivals [40]. Therefore the assumption that classical ergodicity and mixing dominate the quantum evolution is no longer valid. The quantum system at a quantum resonance becomes solvable in the sense defined by Calogero [41], in contrast to the trivial integrability resulting from the linearity of quantum mechanics. This results in a behavior similar to that found for the quantization of a classically integrable system. A detailed discussion is beyond the scope of this paper but is closely related to Ref. [42].

B. Integrable case

Let us now turn to a classically near-integrable case. We choose the kick strength $K=0.5$. The resulting Poincaré plot with a richly structured phase space of stable trajectories is depicted in Fig. 5(a). We therefore expect the fidelity to depend significantly on the choice of the initial state.

1. Momentum eigenstates

In order to highlight this dependence we present first two limiting cases of momentum eigenstates. In Fig. 5(c) we

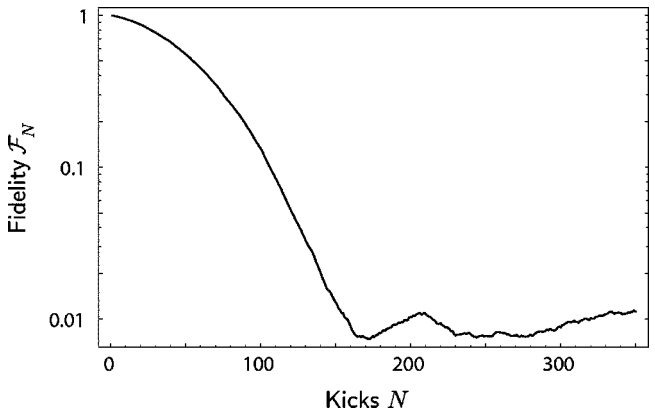

FIG. 4. Fidelity decay for a quantum resonance. For $\hbar=4\pi/100$ the fidelity $\mathcal{F}_N$ shows a Gaussian decay although the parameters are with $K=10$ in the classically nonintegrable regime. For the plot we chose an initial state $|\rho=0\rangle$ and a perturbation $\delta=0.01$.

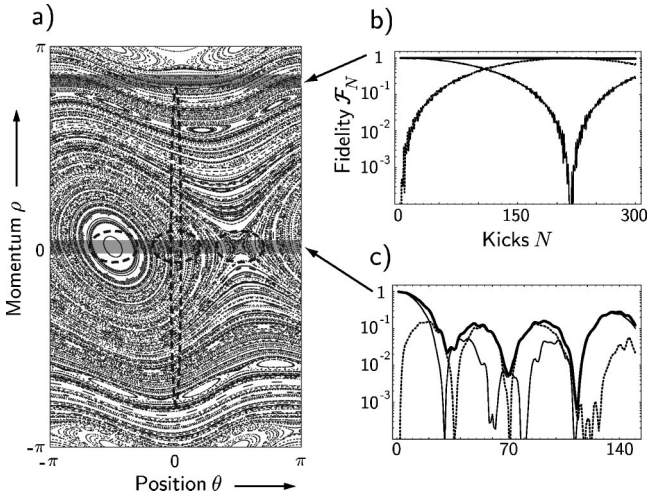

FIG. 5. Fidelity decay in the integrable regime. The Poincaré plot shown in (a) depicts the richly structured classical phase space for $K=0.5$ which consists of only stable trajectories. Again we choose two initial momentum eigenstates $|\rho=0\rangle$ and $|\rho=13\hbar\rangle$ with $\hbar=0.2$. The uniform phase space distribution corresponding to their classical limit is given by the shaded areas in (a). The dashed ellipses represent Gaussian-like states which we used as initial states for the fidelity decay shown in Figs. 7 and 8, where the dashed lines show the contour at half maximum. In (b) the distribution lies in an area of almost flat trajectories leading to an stable dynamics as suggested by the nearly constant fidelity $\mathcal{F}_N$ denoted by the thick horizontal line. The square of the real (thin line) and imaginary part (dotted line) show distinct variation and only their sum is balanced out to a constant. In (c), where the initial distribution lies in an area of closed trajectories, the fidelity shows initially a Gaussian decay and ends in bounded oscillations. This behavior we find also in the real and imaginary part where the initial decay is governed by the real part.

have chosen an initial state $|l\hbar\rangle$ with $l=0$ which is embedded in a region of phase space dominated by closed trajectories. In contrast in Fig. 5(b) we select a state with $l=13$ covering a phase-space region of almost flat trajectories, which mimic the shape of momentum eigenstates. This difference in the initial states is reflected in the time evolution of the corresponding fidelities. In the first case we find the Gaussian decay predicted by Eq. (11) followed by an oscillatory behavior. The second case is characterized by an almost constant fidelity.

In a semiclassical picture this can be easily understood: The initial phase-space distribution, shaded in the Poincaré plot, Fig. 5(a), evolves according to the classical trajectories. The fidelity can then be interpreted as the overlap between two such distributions evolving along slightly different trajectories corresponding to K and $K+\delta$. In the case depicted in Fig. 5(c) the distributions circulate with almost constant frequency near the center of the island, which causes the regular oscillations, while the variable frequency in the outer parts cause the Gaussian decay. The almost constant fidelity in Fig. 5(b) suggests that the momentum eigenstate is almost exactly an eigenstate of the Floquet operator. This seems rather obvious, because the flat trajectories do not considerably change the shape of the initial distribution.

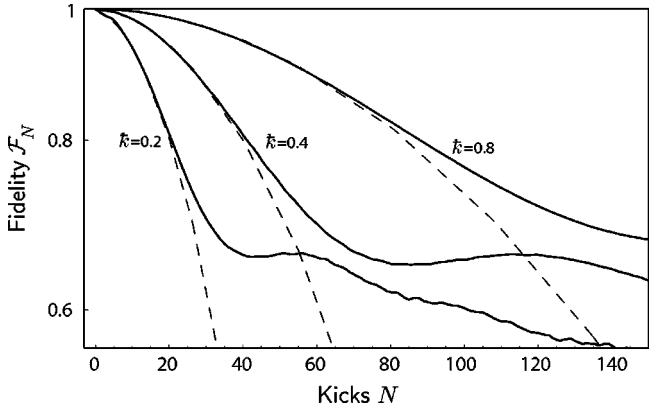

FIG. 6. Fidelity decay averaged over many different initial states in the integrable regime $K=0.5$. The plot shows the Loschmidt echo for three different values of $\hbar$. Initially the decay is purely Gaussian and finally saturates to a constant which reflects the nonvanishing correlations in the integrable system. Note that the curves result from averaging fidelities of types shown in Fig. 5(b) and 5(c), that is, they consist of rapidly and almost nondecaying contributions. The dotted lines represent fitted Gaussian curves.

As in the chaotic case we include in Fig. 5 the square of the real and imaginary parts of the fidelity amplitude. Again we find that the real part determines the short-time decay which is now Gaussian. The oscillations in the fidelity for the initial state with $l=0$ originate from both the real and imaginary parts. For the approximate Floquet eigenstate with $l=13$ we find that the decay of the real part is balanced by an increase of the imaginary part as they oscillate with opposite phase. This results in an almost constant fidelity.

2. Mixed states

In order to average out the dependence on different initial states in Fig. 6 we use again a mixed state which consists of many equally weighted momentum eigenstates $|l\hbar\rangle$. We compare the averaged fidelity for the three different values of $\hbar=0.2$, $\hbar=0.4$, and $\hbar=0.8$. In contrast to the chaotic case we find now a Gaussian decay of the fidelity, in agreement with the theoretical prediction given in Eq. (11). We have fitted Gaussians $\beta' \exp[-N^2/\sigma^2]$ to the fidelity decay and found the ratio of width to be $1:2.07:3.91$ which is in good agreement with the prediction of Eq. (11). This agreement indicates that $\tilde{\mathcal{C}}$ does not depend strongly on the parameters $\hbar$.

In the chaotic case we have seen a deviation from Eq. (9) due to the fact that the Hilbert space becomes small for large $\hbar$ as a consequence of localization. A similar deviation from Eq. (11) does not occur because the correlation functions saturate at higher values than those that result from the dimension of these spaces.

3. Pure Gaussian initial states

So far we have only discussed momentum eigenstates and their incoherent superpositions. We now address the question of stability of coherent superpositions using Gaussian states,

$$|\psi_0\rangle = \mathcal{N}\sum_{\rho} \exp[-\rho^2/(4\sigma_\rho^2)]|\rho\rangle, \tag{13}$$

in momentum space with the normalization constant $\mathcal{N}$. We calculate the fidelity decay for the two different values σ_ρ

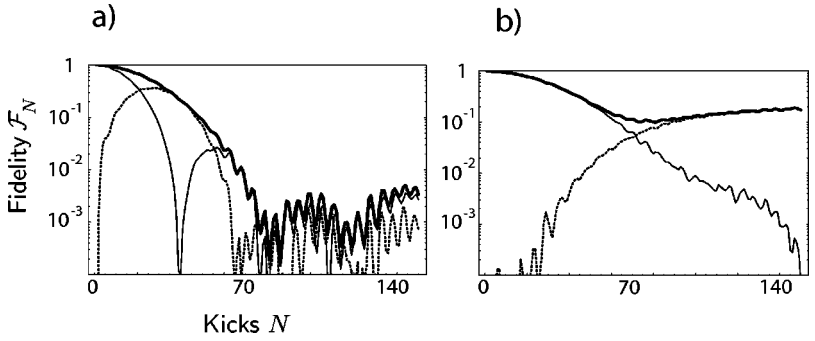

FIG. 7. Fidelity decay for Gaussian-like initial states. In (a) we show the result for the initial state, Eq. (13), with $\sigma_\rho=\hbar$. This corresponds to an almost equal position and momentum distribution centered at the origin of phase space, as illustrated in Fig. 5(a) by the egg-shaped ellipse. The fidelity decay for an initial state with broad momentum distribution and localized in position ($\sigma_\rho=10\hbar$) is shown in (b). We have again symbolized this state by the stretched ellipse in Fig. 5(a). In both plots we show again the fidelity (thick line) and the square of the real (thin line) and imaginary part (dotted line). The parameters are $K=0.5$, $\hbar=0.2$, and $\delta=0.02$.

$=\hbar$ and $\sigma_\rho=10\hbar$ for the momentum width. The corresponding distributions in phase space are represented by the two dashed ellipses centered at zero momentum and position in Fig. 5(a). The resulting fidelity, as well as its squared real and imaginary parts are shown in Fig. 7. In both cases we again find the expected Gaussian decay. However, only in the second case this decay originates from the real part, whereas the imaginary part defines the plateau. In the first case both the decay and the plateau result from a complicated interplay of real and imaginary part.

4. Plateaus and oscillations

For different states the fidelity after many kicks results either in plateaus or in oscillations, where the latter are washed out in the incoherent averages. For momentum eigenstates shown in Fig. 5 the time at which the fidelity deviates from the Gaussian decay law varies from around 40 kicks to infinity, with an upper bound of the fidelity in that range from near unity to 10^{-1}. For coherent states (Fig. 7) we find a time of roughly seventy kicks and after the decay the fidelity varies from 10^{-1} to 10^{-2}.

The oscillations apparent in Figs. 5(c) and 7(a) are qualitatively understood in terms of the classical frequencies included in the corresponding states. The oscillations around the mean value of the momentum eigenstate, Fig. 5(c), display one basic frequency. Similarly, the coherent state with $\sigma_\rho=\hbar$ is determined by the same basic frequency as seen in the $l=0$ momentum eigenstate. However, the beatings of higher frequency components blot out the ground frequency entirely indicating the central role of interferences. Yet the real and imaginary parts individually still display this frequency quite clearly. The coherent state underlying Fig. 7(b) apparently contains so many different frequencies, that it behaves quite similar to an incoherent superposition shown in Fig. 6, though the near eigenstates of the Floquet operator are represented with less weight than in the incoherent superposition. The height of the plateau in the incoherent superposition of momentum states is simply explained by the large portion of momentum eigenstates that are almost eigenfunctions of the Floquet operator.

5. Stable and unstable fixed point

We conclude our considerations of the integrable regime by inspecting two special initial states which have very non-generic behavior. Indeed, we place a Gaussian state, Eq. (13), at the center of the integrable island, i.e., at the point $(\theta=-\pi/2,\rho=0)$ shown as dashed ellipse in Fig. 5(a), and another Gaussian state exactly at the principal unstable fixed point $(\pi/2,0)$. As discussed above, the former is precisely the kind of state used by Peres and whose unsurprising behavior can be seen in Fig. 8(a). Rather more interesting is the second case shown in Fig. 8(b). We presume the regular behavior of the fidelity resulting from the fact that the Gaussian wave packet covers not only the hyperbolic fixed point, but also its surrounding. Thus the fast irregular oscillations follow from the unstable fixed point whereas the slow enveloping oscillations are reminiscent of the elliptic trajectories. We shall not go into more details, but rather refer to the extensive, though probably not exhaustive discussion of such a situation in Ref. [43]. There, the authors discuss dynamics near the top of a repulsive oscillator, which is the classical example of a hyperbolic point of this type.

C. Dependence on the kick strength and soft chaos

So far we have analyzed the stability of quantum motion near the two limiting cases where the phase-space portrait was globally chaotic or near integrable. Although the theory presented in Sec. III makes no statement about the intermediate regime, we complete our investigations with numerical results. We choose $\hbar=0.1$ and calculate the fidelity $\mathcal{F}_N$ for five different values of K reaching from global chaos to situations where the Poincaré plot shows stable islands, as depicted in the inset of Fig. 9. We focus on the $|l\hbar=0\rangle$ momentum eigenstate localized in a region of phase space where we expect the primary islands to appear in the Poincaré plot. For the K values ($K=12$, 9, 8, and 7), all corresponding to the near chaotic regime, the decay is exponential as expected. However, the slope of the decay is not a monotonic function of K. For the K value $K=3$, where the surface of section shows stable islands in phase space the decay can be characterized by two distinct features. It behaves exponentially on a longer time scale whereas it shows oscillations on a shorter one. In the short-time regime we recognize the Gaussian decrease typical for the integrable case. On the longer time scale the exponential decay is still present on

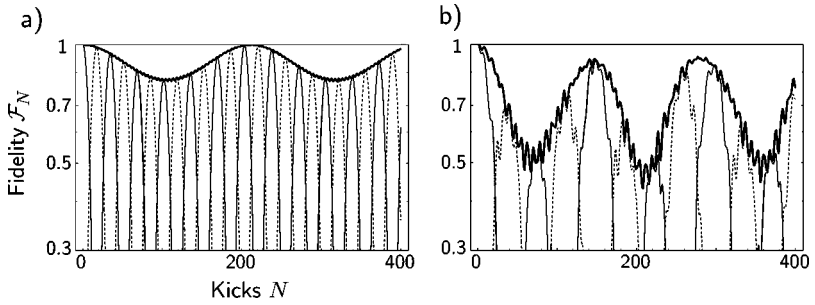

FIG. 8. Fidelity at stable and unstable fixed points. Shown are the fidelity $\mathcal{F}_N$ (thick line) and the square of the real (thin line) and imaginary part (dotted line) of the fidelity amplitude as a function of the kick number N. In a) we have placed a Gaussian state of width $\sigma_\rho=\hbar$ at the center of the stable island $(-\pi/2,0)$. As expected, the fidelity displays oscillations corresponding to the classical frequencies. In contrast, in (b) the Gaussian state is placed at the unstable fixed point $(\pi/2,0)$ and shows highly nongeneric behavior. As parameters we chose $K=0.5$ and $\hbar=0.2$.

average. Therefore from Fig. 9 we can conclude that in the intermediate regime characteristics of both limiting cases are present.

V. ECHO EXPERIMENTS WITH ATOMS

The kicked rotor in its realization of a kicked particle can be experimentally modeled by an atom in a standing light wave and is nowadays routinely implemented in many labs [30,31]. Typically such an experiment consists of an atom of mass M where two electronic states with level spacing ω_0, denoted by the ground state $|1\rangle$ and the excited state $|e\rangle$, are driven by two counterpropagating laser fields. The dipole $\vec{\mu}$ of this transition is coupled to the electromagnetic field $\vec{E}(x,t)=\mathcal{E}\vec{\epsilon}\cos(k_L x+\varphi_L)e^{-i\omega t}+\text{c.c.}$ of the lasers with wave number k_L, frequency ω, complex amplitude $\mathcal{E}$, polarization $\vec{\epsilon}$, and phase φ_L. The Hamiltonian describing this interaction reads in rotating wave approximation

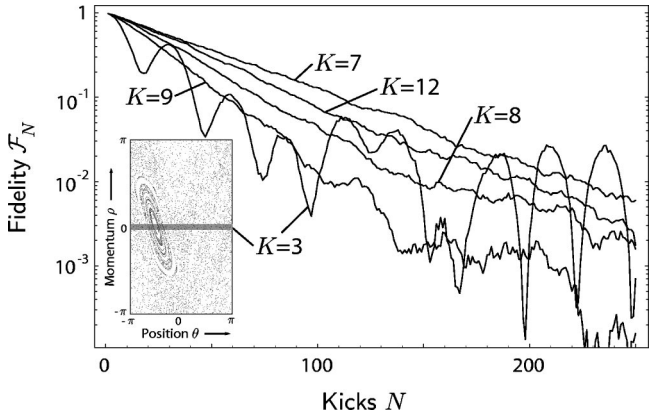

FIG. 9. Fidelity decay approaching the intermediate regime. Shown is the decay of the fidelity $\mathcal{F}_N$ for five different values of K, constant $\hbar=0.1$, and $|l\hbar=0\rangle$. For $K=12$, 9, 8, and 7, that is, for globally chaotic phase space, the decay is exponential as expected, but no clear trend for the decay length can be recognized. For $K=3$ where the phase space shows stable islands (see inset) the decay is characterized by both the exponential decay and oscillations.

$$\hat{H}_{\text{int}}=\frac{\hat{p}^2}{2M}+\hbar\omega_0|e\rangle\langle e|+\left[\frac{\hbar\Omega}{2}\cos(k_L x+\varphi_L)e^{-i\omega t}|e\rangle\langle 1|+\text{H.c.}\right]$$

with the Rabi frequency $\Omega=(\vec{\mu}\cdot\vec{\epsilon})\mathcal{E}/\hbar$. A large detuning $\Delta=\omega_0-\omega$ allows us to adiabatically eliminate the excited state $|e\rangle$ leading to the Hamiltonian

$$\hat{H}_1=\frac{\hat{p}^2}{2M}+\hbar\kappa_1[\sin(2k_L x)+1]\delta_T(t) \tag{14}$$

for the ground state $|1\rangle$ in a frame rotating with the laser frequency. Here we introduced the interaction strength $\kappa_1=\Omega^2/(8\Delta)$ and chose the phase φ_L appropriately. Moreover, the periodic kicks theoretically described by the train of δ functions in Eq. (14) can be approximately realized by rapidly switching on and off the laser fields with period T. Therefore the Hamiltonian Eq. (14) corresponds to the Hamiltonian of the kicked rotor, Eq. (1), in its realization of a kicked atom. The additional constant potential leads only to a global phase factor.

In order to measure the Loschmidt echo an analog setup can be applied if we additionally make use of atom interferometry [23,24,33]. For this reason we take again an atom with excited electronic state $|e\rangle$ but two hyperfine ground states $|1\rangle$ and $|2\rangle$ separated by the hyperfine splitting ω_{hf}, as illustrated in Fig. 10. Following the same procedure as above for large detuning Δ we can again eliminate the excited level and find for the two ground states the Hamiltonian $\hat{H}_g=\hat{H}_1|1\rangle\langle 1|+\hat{H}_2|2\rangle\langle 2|$ with

$$\hat{H}_2=\frac{\hat{p}^2}{2M}+\hbar\omega_{\text{hf}}+\hbar\kappa_2[\sin(2k_L x)+1]\delta_T(t). \tag{15}$$

Here we analogously defined

$$\kappa_2=\frac{\Omega^2}{8(\Delta+\omega_{\text{hf}})}=\kappa_1-d$$

where $d=\kappa_1\omega_{\text{hf}}/(\Delta+\omega_{\text{hf}})$. We mention that the physical quantity d is connected with the scaled perturbation, introduced in Sec. III, via $\delta=\hbar d(\kappa_0^2T^2/M)$.

The motional state of an atom prepared in an internal superposition of states $|1\rangle$ and $|2\rangle$ propagates in two different

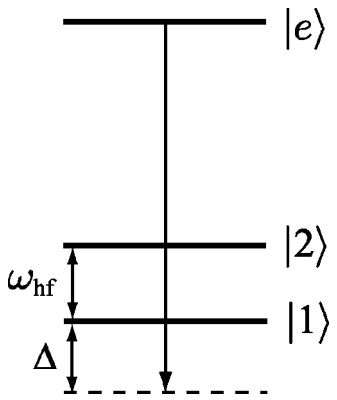

FIG. 10. Level scheme for the measurement of the Loschmidt echo. A classical laser drives the transitions $|e\rangle \leftrightarrow |1\rangle$ and $|e\rangle \leftrightarrow |2\rangle$ of a three-level atom with excited electronic state $|e\rangle$ and two hyperfine ground states $|1\rangle$ and $|2\rangle$ which have a level spacing of $\omega_{\rm hf}$. The laser is detuned by Δ from the transition $|e\rangle \leftrightarrow |1\rangle$ and by $\Delta + \omega_{\rm hf}$ from the transition $|e\rangle \leftrightarrow |2\rangle$.

potentials described by the Hamiltonians $\hat{H}_1$ and $\hat{H}_2$, Eqs. (14) and (15), respectively. Indeed, this is exactly the situation we need to realize a Loschmidt-echo experiment with perturbation d.

We are now in the position to measure the fidelity

$$\mathcal{F}_N = |\tilde{f}_N|^2 = |\langle \psi_0 | \hat{U}_2^{-N} \hat{U}_1^N | \psi_0 \rangle|^2$$

introduced in Eq. (6), where $\hat{U}_i$ describes the time evolution with the Hamiltonian $\hat{H}_i$. For this purpose one has to prepare the atom in a superposition of the internal states $|1\rangle$ and $|2\rangle$ leading to the initial state

$$|\Psi\rangle = \frac{1}{\sqrt{2}}[|1\rangle + |2\rangle]|\psi_0\rangle$$

of the composite system of internal and external degrees of freedom. Here $|\psi_0\rangle$ represents the initial state of the center-of-mass motion. The time evolution as described above leads to the state

$$|\Psi_N\rangle \equiv |\Psi(t = NT)\rangle = \frac{1}{\sqrt{2}}[|1\rangle|\psi_N\rangle + |2\rangle|\phi_N\rangle].$$

From this state the fidelity can be extracted by determining the probability $W_N(\theta) \equiv \int dx |\langle j(\theta)|\langle x|\Psi_N\rangle|^2$ to find the atom in the internal state $|j(\theta)\rangle \equiv (1/\sqrt{2})[|1\rangle + e^{-i\theta}|2\rangle]$. Here we used the position states $|x\rangle$ in order to trace over the external degrees of freedom. We find

$$W_N(\theta) = \frac{1}{2}(1 + \mathrm{Re}[e^{-i\theta}\langle \phi_N|\psi_N\rangle])$$

from which we can finally calculate the real and imaginary part of the fidelity amplitude

$$\mathrm{Re}\,\tilde{f}_N = 2W_N(0) - 1,$$

$$\mathrm{Im}\,\tilde{f}_N = 2W_N(\pi/2) - 1.$$

These results provide us with the fidelity

$$\mathcal{F}_N = (\mathrm{Re}\,\tilde{f}_N)^2 + (\mathrm{Im}\,\tilde{f}_N)^2. \tag{16}$$

Due to the constant potential terms in the Hamiltonians $\hat{H}_1$ and $\hat{H}_2$, Eqs. (14) and (15), the measured fidelity amplitude $\tilde{f}_N$ picks up a constant phase factor $\exp[-i(\omega_{\rm hf} - d)N]$. Thus the desired fidelity amplitude as defined in Eq. (6) is related to the measured fidelity amplitude via

$$f_N = e^{i(\omega_{\rm hf} - d)N}\tilde{f}_N.$$

We now turn to the discussion of a possible experimental implementation. The setup is similar to previous experiments using sodium atoms [30]. We consider the D_2 transition of sodium. The hyperfine levels $3^2S_{1/2}$, $F=1$ and $3^2S_{1/2}$, $F=2$ with a level splitting of approximately 1.77 GHz serve as the ground states $|1\rangle$ and $|2\rangle$. The exited state $|e\rangle$ can be chosen to be the $3^2P_{3/2}$ state. If the interaction laser is tuned 2 THz from resonance (to the blue) of the D_2 line, then the two hyperfine components would experience a potential with fractional difference of about $\delta/K = 0.001$ [48].

In order to create the initial superposition of the states $|1\rangle$ and $|2\rangle$ we apply a Raman pulse which has to be copropagating to avoid momentum change. The time evolution is realized by applying laser pulses with the driving lasers in order to create the momentum kicks. For the readout we apply another $\pi/2$ pulse in the same way as for the preparation such that we have a sequence of two $\pi/2$ pulses with an accumulated phase difference of θ between the two states $|1\rangle$ and $|2\rangle$. The final measurement of the population in the hyperfine states provides us with the real or imaginary part of the fidelity amplitude depending on the phase difference $\theta = 0$ or $\theta = \pi/2$. For details on the experimental controllability of the phase difference θ and the state-selective measurement we refer to Refs. [44,45]. The experiment has to be repeated with the other choice for θ in order to measure the complete fidelity $\mathcal{F}_N$, Eq. (16).

VI. CONCLUSIONS

We have studied the stability of the quantum kicked rotor under perturbations of the Hamiltonian. As a measure of the influence of the perturbation we have used the fidelity in a Loschmidt-echo situation, i.e., we considered the quantum-mechanical overlap of two initially identically prepared states propagated under two slightly different Hamiltonians. We have found good agreement with the theoretical predictions valid for the initial stage of the time evolution. In particular, we distinguished between a classically chaotic and integrable regime and numerically confirmed the theoretically expected decay laws, namely an exponential and a Gaussian decay for the chaotic and integrable case, respectively. Discrepancies from the theoretical predictions can also be distinguished, and have been attributed to the effect of dynamical localization emerging in the model under consideration. Moreover, we also discussed the long-time behav-

ior of the fidelity decay in its dependence on different initial states. Clear signatures of the structure imprinted by classical dynamics on phase space appear. We also briefly considered the special case of quantum resonances and investigated the transient regime between integrability and global chaos.

We additionally emphasize that our results are in agreement with Refs. [7,35]. Both papers predict a wide variation of the fidelity for pure states or states which average over members of some basis. Our present study confirms these claims for the example of the kicked rotor. In contrast to what might be concluded from the title of Ref. [35], we have found that such averages over a specific basis will not provide unique information about quantum chaos, a fact, that can also be inferred from the results of Ref. [35] for two different bases in integrable situations. Insensitivity to the choice of a basis might be some indicator of chaos, but is certainly not a practical test since we cannot try out all basis sets. Furthermore, some sensitivity exists also in the chaotic case for short times [46]. We do not present calculations for random states as their experimental realization is by no means obvious. Hence the corresponding claims in Ref. [7] will be difficult to test experimentally.

We conclude by emphasizing that the parameters used in our study correspond to experiments that can be carried out with state-of-the-art technology. Indeed, all ingredients for the proposed experiment based on atom interferometry are already in operation.

ACKNOWLEDGMENTS

We thank T. Prosen and M. Žnidarič for fruitful discussions. This work was stimulated during the Humboldt Kolleg "Entanglement and Decoherence in Quantum Optics and Atomic Physics" at the Centro Internacional de Ciencias, Cuernavaca, Mexico. We are grateful to the Alexander von Humboldt Stiftung for its support. The work of W.P.S. and M.G.R. is made possible by the Max Planck Preis. M.G.R. acknowledges support from the R.A. Welch Foundation. Support by CONACyT Grant No. 41000-F and DGAPA Grant No. 100803 is acknowledged by T.H.S.

[1] L. Boltzmann, Ann. Phys. **57**, 773 (1896); J. Loschmidt, Wiener Ber. **73**, 128 (1876).
[2] W. Thompson, Proc. R. Soc. Edinburgh **8**, 325 (1874).
[3] A. Peres, *Quantum Theory: Concepts and Methods* (Kluwer Academic Publishers, Dordrecht, 1995).
[4] A. Peres, Phys. Rev. A **30**, 1610 (1984).
[5] R. A. Jalabert and H. M. Pastawski, Phys. Rev. Lett. **86**, 2490 (2001).
[6] Ph. Jacquod, P. G. Silvestrov, and C. W. J. Beenakker, Phys. Rev. E **64**, 055203(R) (2001).
[7] T. Prosen and M. Žnidarič, J. Phys. A **35**, 1455 (2002); T. Prosen, T. H. Seligman, and M. Žnidarič, Prog. Theor. Phys. Suppl. **150**, 200 (2003).
[8] N. R. Cerruti and S. Tomsovic, J. Phys. A **36**, 3451 (2003); **36**, 11 915 (2003).
[9] F. M. Cucchietti, D. A. R. Dalvit, J. P. Paz, and W. H. Zurek, Phys. Rev. Lett. **91**, 210403 (2003).
[10] T. Gorin, T. Prosen, and T. H. Seligman, New J. Phys. **6**, 20 (2004).
[11] T. Prosen and M. Žnidarič, New J. Phys. **5**, 109 (2003).
[12] B. V. Chirikov, Phys. Rep. **52**, 263 (1979).
[13] F. M. Cucchietti, C. H. Lewenkopf, E. R. Mucciolo, H. M. Pastawski, and R. O. Vallejos, Phys. Rev. E **65**, 046209 (2002).
[14] G. Benenti and G. Casati, Phys. Rev. E **65**, 066205 (2002).
[15] R. Schack and C. M. Caves, Phys. Rev. E **53**, 3387 (1996).
[16] Weng-ge Wang and Baowen Li, Phys. Rev. E **66**, 056208 (2002); Weng-ge Wang, G. Casati, and Baowen Li, *ibid.* **69**, 025201(R) (2004).
[17] L. Benet, T. H. Seligman, and H. A. Weidenmüller, Phys. Rev. Lett. **71**, 529 (1993).
[18] D. Cohen, Ann. Phys. (N.Y.) **283**, 175 (2000).
[19] L. Kaplan, New J. Phys. **4**, 90 (2002).
[20] E. L. Hahn, Phys. Rev. **80**, 580 (1950).
[21] H. M. Pastawski, P. R. Levstein, G. Usaj, J. Raya, and J. Hirschinger, Physica A **283**, 166 (2000).
[22] S. Zhang, B. H. Meier, and R. R. Ernst, Phys. Rev. Lett. **69**, 2149 (1992).
[23] S. A. Gardiner, J. I. Cirac, and P. Zoller, Phys. Rev. Lett. **79**, 4790 (1997); **80**, 2968 (1998).
[24] S. Schlunk, M. B. d'Arcy, S. A. Gardiner, D. Cassettari, R. M. Godun, and G. S. Summy, Phys. Rev. Lett. **90**, 054101 (2003).
[25] H.-J. Stoeckmann (private communication).
[26] G. Casati, B. V. Chirikov, J. Ford, and F. M. Izrailev, Lect. Notes Phys. **93**, 334 (1979).
[27] F. M. Izrailev, Phys. Rep. **196**, 299 (1990).
[28] S. Fishman, D. R. Grempel, and R. E. Prange, Phys. Rev. Lett. **49**, 509 (1982).
[29] F. L. Moore, J. C. Robinson, C. F. Bharucha, Bala Sundaram, and M. G. Raizen, Phys. Rev. Lett. **75**, 4598 (1995).
[30] M. G. Raizen, Adv. At., Mol., Opt. Phys. **41**, 43 (1999).
[31] M. B. d'Arcy, R. M. Godun, M. K. Oberthaler, D. Cassettari, and G. S. Summy, Phys. Rev. Lett. **87**, 074102 (2001).
[32] H. Ammann, R. Gray, I. Shvarchuck, and N. Christensen, Phys. Rev. Lett. **80**, 4111 (1998).
[33] M. Bienert, F. Haug, W. P. Schleich, and M. G. Raizen, Phys. Rev. Lett. **89**, 050403 (2002).
[34] M. Žnidarič, Ph.D. thesis University of Ljubljana (Slovenia) Faculty of Mathematics and Physics, Physics Department, 2004, also available at quant-ph/0406124.
[35] J. Emerson, Y. S. Weinstein, S. Lloyd, and D. G. Cory, Phys. Rev. Lett. **89**, 284102 (2002).
[36] F. Haake, *Quantum Signatures of Chaos* (Springer, Heidelberg, 2000).
[37] L. E. Reichl, *The Transition to Chaos* (Springer, Berlin, 1992).
[38] D. L. Shepelyansky, Physica D **28**, 103 (1987), and references therein.
[39] F. M. Izrailev and D. L. Shepelyansky, Theor. Math. Phys. **43**, 553 (1980).
[40] W. P. Schleich, *Quantum Optics in Phase Space* (Wiley-VCH,

Berlin, 2001).
[41] M. Bruschi and F. Calogero, J. Nonlinear Math. Phys. **7**, 303 (2000).
[42] S. Wimberger, I. Guarneri, and S. Fishman, Nonlinearity **16**, 1381 (2003); Phys. Rev. Lett. **92**, 084102 (2004).
[43] R. Blume-Kohout and W. H. Zurek, Phys. Rev. A **68**, 032104 (2003).
[44] M. Kasevich and S. Chu, Phys. Rev. Lett. **67**, 181 (1991).
[45] M. Kasevich and S. Chu, Phys. Rev. Lett. **69**, 1741 (1992).
[46] T. Prosen and M. Žnidarič, Phys. Rev. Lett. **94**, 044101 (2005).
[47] Strictly speaking, one has to assume classical ergodicity and fast mixing of the system. Typically this corresponds to the chaotic case. For more details consult Ref. [7].
[48] Note that in the given example using sodium atoms, a detuning of 2 THz from the D_2 transition means that also the D_1 transition separated from D_2 by about 0.5 THz contributes to the Stark shift. For the numbers presented in the example the relative difference δ/K does not change significantly since also K alters. In any case, however, we can simply readjust the laser detuning Δ to achieve the desired coupling strengths.